Supplement of The Cryosphere, 19, 713–730, 2025
https://doi.org/10.5194/tc-19-713-2025-supplement

The Cryosphere Open Access EGU

Supplement of

Amundsen Sea Embayment accumulation variability measured with global navigation satellite system interferometric reflectometry

Andrew O. Hoffman et al.

Correspondence to: Andrew O. Hoffman (aoh2111@columbia.edu)

S1 Introduction

Here we provide additional information on comparisons between accumulation from reanalysis products at the sites of the GNSS receivers, composite anomalies, the significance testing for composite anomalies, and the Rossby wave calculations.

S2 Comparison between reanalysis and GNSS-IR

Using the nearest grid cell of different reanalysis products (MERRA-2 and ERA-5) and high-resolution climate simulations (RACMO-2), we compare simulated accumulation rates with measured accumulation rates (Gelaro et al., 2017; Hersbach et al., 2020; van Wessem et al., 2018).

S3 ERA5 composite analysis

S3.1 Anomalies

Anomalies were calculated by subtracting the historical seasonal means for the observational period (2009–2022) from the respective environmental variable for each individual JJA and DJF snowfall event (including the days building up to the event).

S3.2 Significance testing

A difference of means test was used to determine the significance of extreme snow accumulation at the GNSS sites associated with and without blocking present and tested at the 95% level. We use the permutation test to assess the significance of the seasonal changes in the accumulation climatology at each site. The null hypothesis of this experiment is that the observed seasonality (or periodic pattern) is not statistically significant and could be attributed to Gaussian distributed noise. We first compute the autocorrelation function for the original climatological mean and standard deviation of the accumulation time series. We then shuffle the data (randomly permuting the daily accumulation rates independently). This breaks any existing temporal structure or seasonality of the data. We then calculate the test statistic for each permutation repeating this process 10,000 times to build a distribution of the maximum autocorrelation values according to the null hypothesis. Special care must be taken in the interpretation of multiple statistical hypothesis tests (i.e. when each of many tests corresponds to a different location; Wilks, 2016). A Student's t-test was used to determine regions where geopotential height, temperature, and Integrated Vapor Transport anomalies are significantly different from zero at the 95% level.

Table S1. Reflector height time series observation summary

site name (GNSS-IR or surface core)	start date	end date	days where accumulation could be extracted or averaged
Kohler (KHLR)	**2010-01-24**	**2019-09-04**	**2231**
Lower Thwaites (LTHW)	**2009-12-12**	**2021-03-08**	**2941**
Upper Thwiates (UTHW)	**2009-01-01**	**2021-03-23**	**3282**
PIGD (Johnson et al., 2018)	2016-01-31	2016-12-19	324
PIG4 (Johnson et al., 2018)	2016-01-30	2016-12-21	327
PIG3 (Johnson et al., 2018)	2016-01-30	2016-12-24	330
PIG2 (Johnson et al., 2018)	2016-01-29	2016-12-26	333
PIG1 (Johnson et al., 2018)	2016-01-28	2016-12-28	336
D115 (Johnson et al., 2018)	2016-01-29	2016-12-20	327
Cavity Camp ADG (Maclennan et al., 2022)	2020-01-29	2020-02-17	19
Channel Camp ADG (Maclennan et al., 2022)	2020-01-29	2020-02-17	19

Table S2. Parameters used in Metropolis-Hastings algorithm that define the inverse methods.

Parameter.(unit if applicable)	Description	label and value if fixed
mast height.(m)	The height of the antenna mast in meters.	6.125
Initial viscosity.(Pa · s)	The viscosity of the snow relates stress due to overburden pressure and near-surface densification between the surface and the base of the anchor.	$\eta = 7.77e^{12}$
Initial density.(kg/m^3)	Surface snow density	$\rho_{snow} = 300$
gravitational constant.(m/s^2)	gravitational acceleration	$g = 9.8$
objective functional	metric used to select the best-fit solution.	ϕ
modeled reflector height.(m)	modeled reflector height at time $t = k$	R_{out_k}
observed reflector height.(m)	observed reflector height at time $t = k$	R_{obs_k}
model step for accumulation.(m)	standard deviation of Gaussian distribution used to select potential accumulation at each step	$\sigma = 0.01$
model step for snow density.(kg/m^3)	standard deviation of Gaussian distribution used to select potential snow density	$\sigma = 3$
model step for viscosity.(Pa · s)	standard deviation of Gaussian distribution used to select potential snow viscosity	$\sigma = 1e10$
Regularization parameter	Parameter that controls the false positive acceptance rate of model parameters (See Equation 6)	$B = 1e5$

Table S3. Reflector height time series observation summary

	MERRA-2	**RACMO-2**	**ERA-5**
Kohler (KHLR)	0.305	0.301	0.325
Lower Thwaites (LTHW)	0.211	0.156	0.140
Upper Thwiates (UTHW)	0.203	0.216	0.219
MERRA-2	1.0	0.807	0.764
RACMO-2	0.807	1.0	0.690
ERA-5	0.764	0.690	1.0

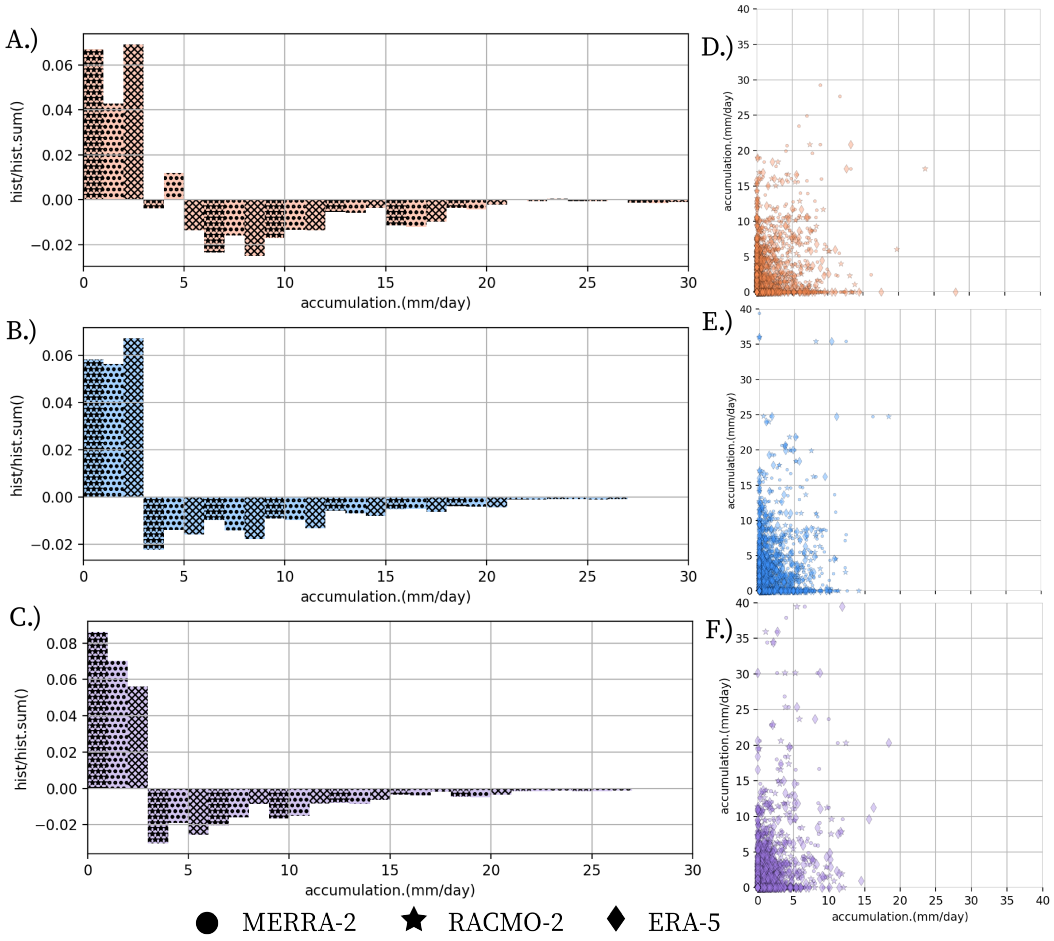

Figure S1. Comparison of MERRA-2 (circles), RACMO-2 (stars), and ERA5 (diamonds) reanalysis products and GNSS-IR derived accumulation histograms of event frequencies for (A) LTHW, (B) UTHW, and (C) KHLR GNSS sites. Histogram difference of reanalysis accumulation and observed accumulation shown in (A-C) are referenced to the reanalysis product (reanalysis product histogram - GNSS-derived accumulation histogram). Accumulation measured with GNSS-IR plotted against accumulation determined from reanalysis products are also shown for (D) LTHW, (E) UTHW, and (F) KHLR GNSS sites.

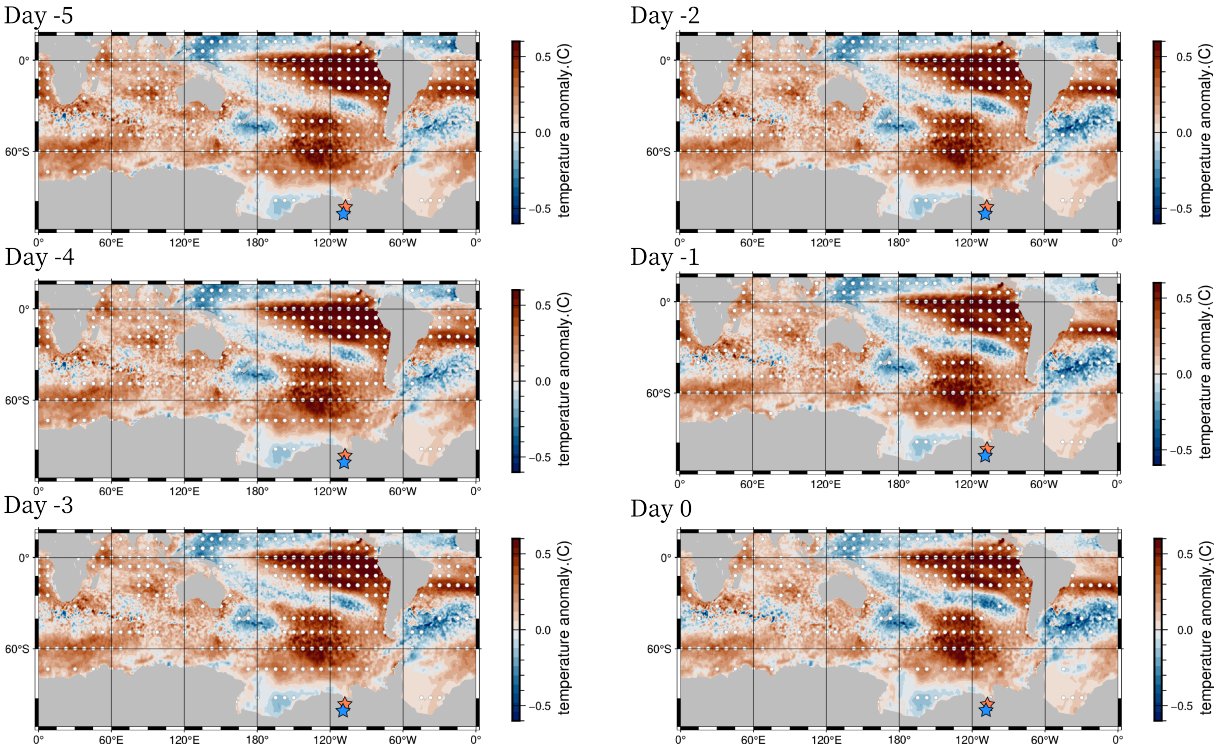

Figure S2. Austral summer sea surface temperature anomalies. Days for each panel indicate the shifted index for composite average prior to (or on) the day of extreme precipitation observed at the GNSS-IR stations located on Thwaites Glacier, which are plotted as orange and blue stars.

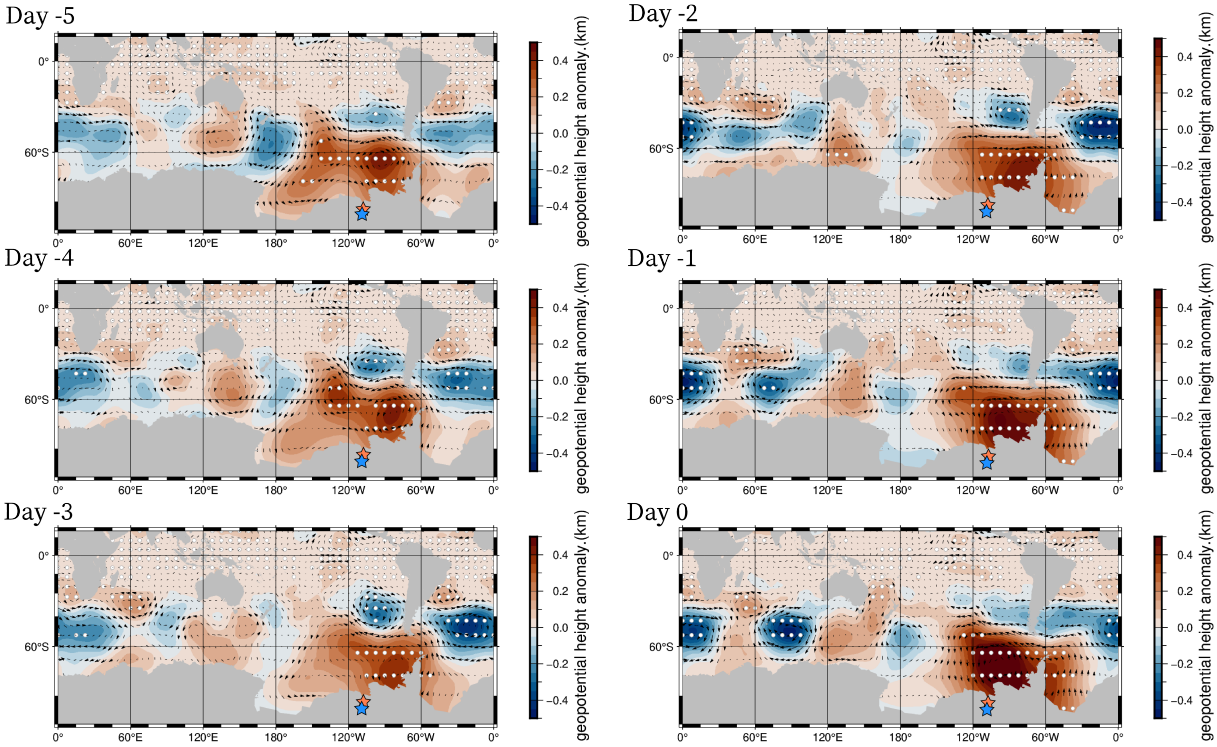

Figure S3. Austral summer geopotential height anomalies at the 500 hPa pressure level. Days for each panel indicate the shifted index for composite average prior to (or on) the day of extreme precipitation observed at the GNSS-IR stations located on Thwaites Glacier, which are plotted as orange and blue stars.

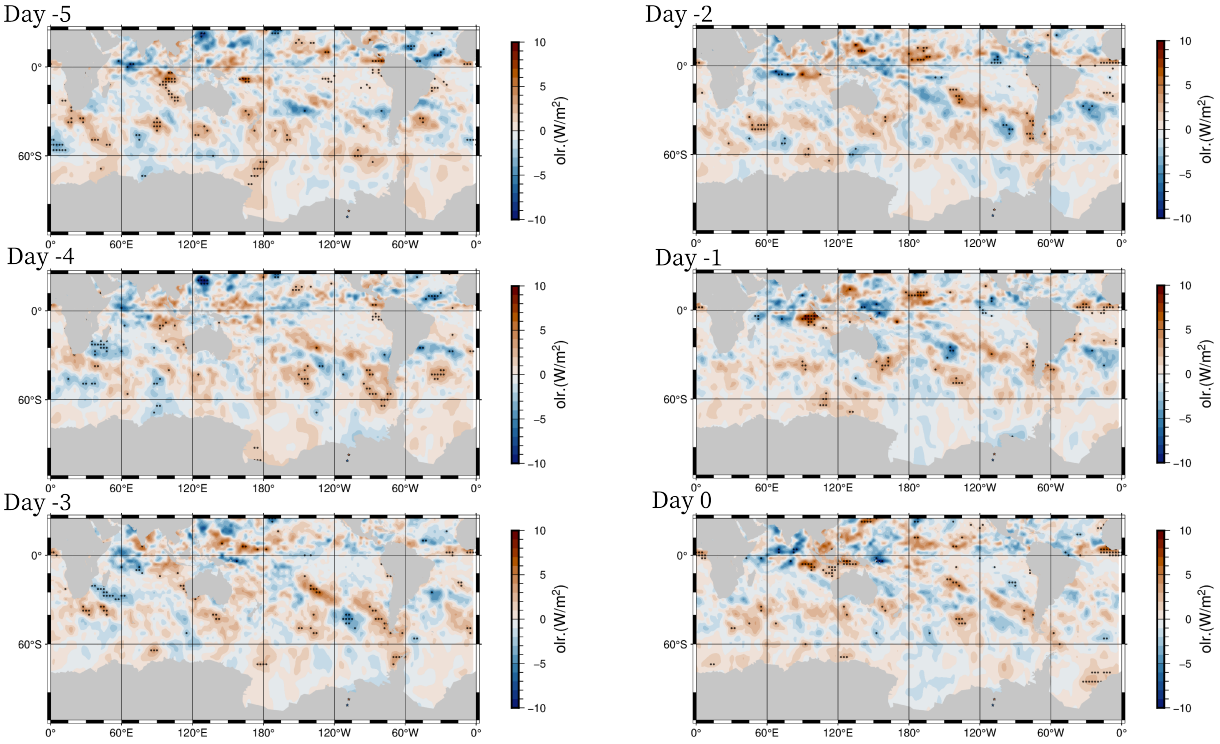

Figure S4. Austral winter Outgoing longwave radiation (OLR) anomalies. Days for each panel indicate the shifted index for composite average prior to (or on) the day of extreme precipitation observed at the GNSS-IR stations located on Thwaites Glacier, which are plotted as orange and blue stars.

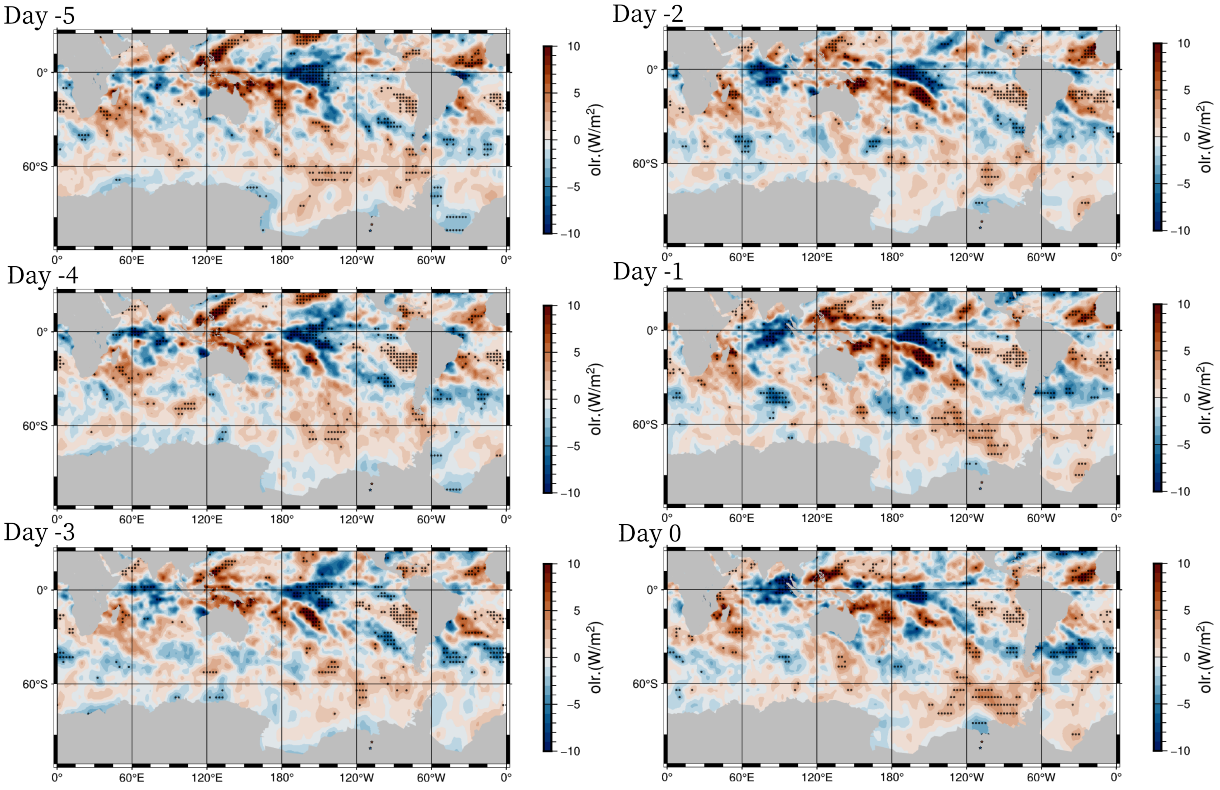

Figure S5. Same as fig. S4 but with austral summer OLR anomalies.

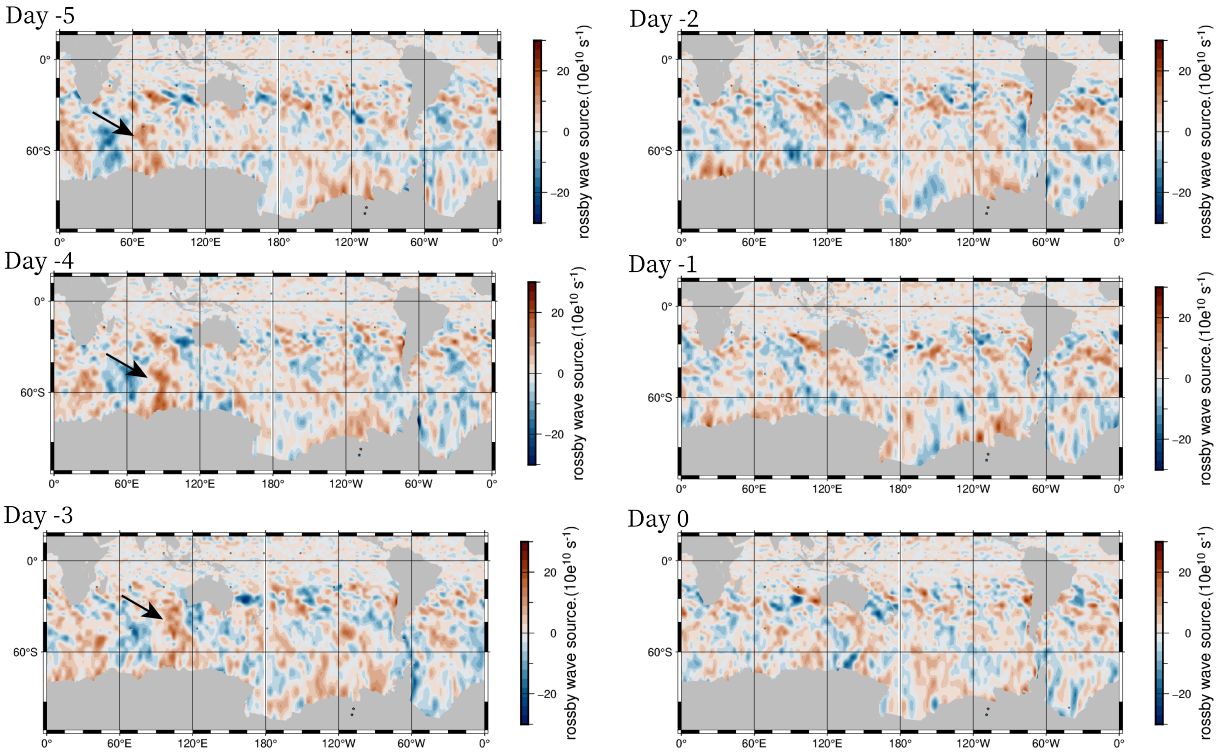

Figure S6. Austral winter Rossby wave source anomalies calculated from 200 hPa winds. Days for each panel indicate the shifted index for composite average prior to (or on) the day of extreme precipitation observed at the GNSS-IR stations located on Thwaites Glacier, which are plotted as orange and blue stars.

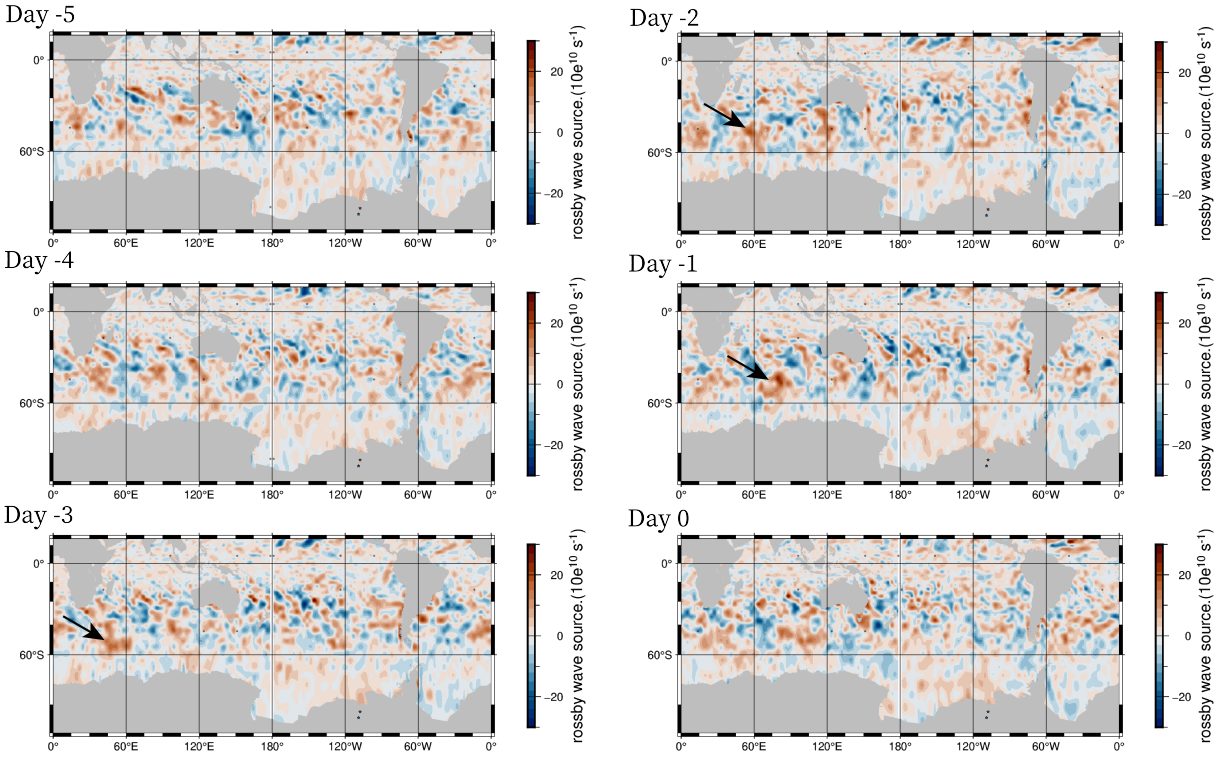

Figure S7. Same as fig. S6 but with austral summer Rossby wave anomalies.

References

Gelaro, R., McCarty, W., Suárez, M. J., Todling, R., Molod, A., Takacs, L., Randles, C. A., Darmenov, A., Bosilovich, M. G., Reichle, R., Wargan, K., Coy, L., Cullather, R., Draper, C., Akella, S., Buchard, V., Conaty, A., da Silva, A. M., Gu, W., Kim, G.-K., Koster, R., Lucchesi, R., Merkova, D., Nielsen, J. E., Partyka, G., Pawson, S., Putman, W., Rienecker, M., Schubert, S. D., Sienkiewicz, M., and Zhao, B.: The Modern-Era Retrospective Analysis for Research and Applications, Version 2 (MERRA-2), Journal of Climate, 30, 5419 – 5454, https://doi.org/https://doi.org/10.1175/JCLI-D-16-0758.1, 2017.

Hersbach, H., Bell, B., Berrisford, P., Hirahara, S., Horányi, A., Muñoz-Sabater, J., Nicolas, J., Peubey, C., Radu, R., Schepers, D., Simmons, A., Soci, C., Abdalla, S., Abellan, X., Balsamo, G., Bechtold, P., Biavati, G., Bidlot, J., Bonavita, M., Chiara, G., Dahlgren, P., Dee, D., Diamantakis, M., Dragani, R., Flemming, J., Forbes, R., Fuentes, M., Geer, A., Haimberger, L., Healy, S., Hogan, R. J., Hólm, E., Janisková, M., Keeley, S., Laloyaux, P., Lopez, P., Lupu, C., Radnoti, G., Rosnay, P., Rozum, I., Vamborg, F., Villaume, S., and Thépaut, J.: The ERA5 global reanalysis, Quarterly Journal of the Royal Meteorological Society, 146, 1999–2049, https://doi.org/10.1002/qj.3803, 2020.

Johnson, J. S., O'Donnell, J. P., and Thomas, E. R.: In situ measurements of snow accumulation in the Amundsen Sea Embayment during 2016, Antarctic Science, 30, 197–203, https://doi.org/10.1017/S0954102018000068, 2018.

Maclennan, M. L., Lenaerts, J. T. M., Shields, C., and Wille, J. D.: Contribution of Atmospheric Rivers to Antarctic Precipitation, Geophysical Research Letters, 49, e2022GL100 585, https://doi.org/10.1029/2022gl100585, 2022.

van Wessem, J. M., van de Berg, W. J., Noël, B. P. Y., van Meijgaard, E., Amory, C., Birnbaum, G., Jakobs, C. L., Krüger, K., Lenaerts, J. T. M., Lhermitte, S., Ligtenberg, S. R. M., Medley, B., Reijmer, C. H., van Tricht, K., Trusel, L. D., van Ulft, L. H., Wouters, B., Wuite, J., and van den Broeke, M. R.: Modelling the climate and surface mass balance of polar ice sheets using RACMO2 – Part 2: Antarctica (1979–2016), The Cryosphere, 12, 1479–1498, https://doi.org/10.5194/tc-12-1479-2018, 2018.

Wilks, D. S.: "The Stippling Shows Statistically Significant Grid Points": How Research Results are Routinely Overstated and Overinterpreted, and What to Do about It, Bulletin of the American Meteorological Society, 97, 2263 – 2273, https://doi.org/https://doi.org/10.1175/BAMS-D-15-00267.1, 2016.